Tukey methods [G. M. Jenkins and D. G. Watts, *Spectral Analysis and its Applications* (Holden-Day, Oakland, CA, 1968)] to the $\delta^{18}O$ anomalies resolves statistically significant (minimum of 80% level) spectral peaks at 12.2-, 8.3-, 5.5-, 3.78-, 2.3-, and 1.7-year periods. The maximum entropy method places these peaks at 11.4, 7.8, 5.5, and 3.5, 2.3, and 1.7 years.

13. We used singular spectrum analysis (SSA) [R. Vautard and M. Ghil, *Physica D* **35**, 395 (1989)] to reconstruct the most energetic modes in the coral record. After the removal of the seasonal cycle and the long-term trend, with a window length of $M = 39$ years, SSA produces two modes in clean quadrature: modes 1 and 2, with a period of 11.8 years, and modes 3 and 4, with a period of 5.3 years (modes with periods greater than 39 years are unresolved). After the further removal of the decadal and interdecadal modes and with a window length of $M = 25$ years, two modes emerge in quadrature: modes 1 and 2, with a period of 5.3 years, and modes 3 and 4, with a period of 3.5 years. The quasi-biennial signal emerges in clean quadrature when a 10-year window length is used. Monte Carlo simulations suggest that all of these modes represent statistically significant (at the 95% confidence level) concentrations of variance. More conventional band-pass filtering yields nearly identical patterns.
14. J. E. Cole *et al.*, *Science* **260**, 1790 (1993).
15. Darwin sea level pressure anomalies were supplied to us by R. Allan of the Commonwealth Scientific and Industrial Research Organization. Pressure anomalies at Darwin lead the Seychelles coral anomalies by 3 to 5 months throughout most of the period of record overlap. However, the zero phase correlation across the entire 3- to 6-year band is 0.79, and cross-spectral estimates suggest that over 80% of the variance in the 3.5- and 5.3-year periods is coherent.
16. A. J. Troup, *Q. J. R. Meteorol. Soc.* **91**, 490 (1965).
17. R. B. Dunbar *et al.*, *Paleoceanography* **9**, 291 (1994).
18. B. Parthasarthy, K. R. Kumar, A. A. Munot, *Proc. Indian Acad. Sci. Earth Planet. Sci.* **102**, 121 (1993).
19. G. A. Meehl, *Science* **266**, 263 (1994).
20. T. P. Barnett, *J. Clim.* **4**, 269 (1991).
21. _____ *Geophys. Res. Lett.* **16**, 803 (1989).
22. M. Latif and T. P. Barnett, *Science* **266**, 634 (1994).
23. R. J. Allan *et al.*, *J. Clim.* **8**, 1853 (1995).
24. R. W. Reynolds and T. M. Smith, *J. Clim.* **7**, 929 (1994).
25. M. Gagan, A. R. Chivas, P. J. Isdale, *Earth Planet. Sci. Lett.* **121**, 549 (1994).
26. R. J. Slutz *et al.*, comprehensive Ocean-Atmosphere Data Set, Release 1 (Climate Research Program, Boulder, CO, 1985).
27. We thank J. Ardai, K. Broad, and A. Hilton for technical support; D. Laredo from the Seychelles Public Utilities Commission and S. Marshall of the Seychelles Ministry of Foreign Affairs, Planning and Environment for facilitating the field work; and M. Moore and D. Schrag and other reviewers for useful discussion. D.E.H. was supported through a Department of Energy–Oak Ridge Institute for Science and Education graduate fellowship. The project itself was sponsored by the National Oceanic and Atmospheric Administration Scripps-Lamont Consortium.

31 January 1997; accepted 30 June 1997

Realization of a Functional Cell for Quantum-Dot Cellular Automata

A. O. Orlov, I. Amlani, G. H. Bernstein, C. S. Lent, G. L. Snider

This paper presents an experimental demonstration of a basic cell of the quantum-dot cellular automata, a transistorless approach to computation that addresses the issues of device density, interconnection, and power dissipation. The device under study was composed of four metal dots, connected with tunnel junctions and capacitors, and operated at <50 mK. Operation was evidenced by switching of a single electron between output dots controlled by a single electron switching in input dots, demonstrating a nonlinear, bistable response.

Achievement of ever higher levels of integration in microelectronics eventually will require a shift from the field-effect transistor (FET)–based paradigm. Scaling of FETs will be limited by unacceptable power dissipation and short-channel effects, which lead to performance degradation. One alternative architecture, quantum-dot cellular automata (QCA) (*1*), is a transistorless approach with quantum dots that addresses the issues of device density, interconnection, and power dissipation. Conventional digital architectures use transistors as current switches to charge and discharge capacitors to the required logic voltage levels. In QCA, logic states are encoded no longer as voltages but rather by the positions of individual electrons. QCA architecture is scalable to molecular levels, and performance actually improves as the size of the device is decreased. The cell presented here operates at cryogenic temperatures, but a molecular-sized QCA cell would function at room temperature.

On the basis of existing technology, a possible realization of a basic QCA cell would be composed of two series-connected metal dots separated by tunneling barriers and capacitively coupled to a second, identical double dot. The dots and associated capacitances are sufficiently small that the system is in the Coulomb blockade regime (*2*) at the temperature of the experiment. If the cell is biased so that there are two excess electrons within the four dots (one excess electron per double dot), those electrons are forced to opposite corners of the four-dot system by Coulomb repulsion. The two possible polarization states of the system represent logic 0 and 1, as indicated in Fig. 1A. Properly arranged, arrays of these basic cells can implement Boolean logic functions (*3*).

We report the experimental demonstration of a functioning QCA cell. Direct measurements of the charging diagram of output dots under the influence of electron switching in input dots, combined with electrometer measurements of output dots, show a controlled polarization change of a QCA cell. Our experimental results show excellent agreement with theory.

The device consists of four Al islands, with input dots D1 and D2 and output dots D3 and D4 (Fig. 1B). The Al-AlO_x-Al tunnel junctions were fabricated on an oxidized Si substrate by a standard electron beam–lithography and shadow evaporation technique (*4*). The area of the junctions is about 60 by 60 nm. The sample was mounted on the cold finger of a dilution refrigerator with a base temperature of 15 mK. Conductances of the double dot and each input dot were measured simultaneously by standard ac lock-in techniques with an excitation voltage of 4 μV at 16 to 40 Hz. A magnetic field of 1 T was applied to suppress the superconductivity of the metal. Typical resistance of a single junction at 1 K was 200 kilohm. Capacitances between gates and islands were determined from the period of the Coulomb blockade oscillations, and values of junction capacitances were extracted from current-voltage measurements (*2*).

A polarization change of the QCA cell requires an electron transfer between dots within each double dot. Gate electrodes force an electron to switch from one dot to the other within the input set of dots, which in turn induces a switch of the other electron in the output dots. This process can best be understood by considering the motion of electrons within one double dot. By measuring the conductance through the double dot as a function of the gate voltages V_C and V_D (Fig. 1C), we can determine the electron charge configuration within the double dot. Current can flow through a double dot only at certain settings of the gate voltages, where the Coulomb blockade is lifted for both dots simultaneously. A contour plot of the measured conductance through a double dot as a function of gate voltages V_C and V_D (Fig. 1D) shows peaks in conductance at triple points, T, which form a hexagonal "honeycomb" (*5*). Each hexagonal cell is delineated by dashed lines in Fig. 1D,

Department of Electrical Engineering, University of Notre Dame, Notre Dame, IN 46556, USA.

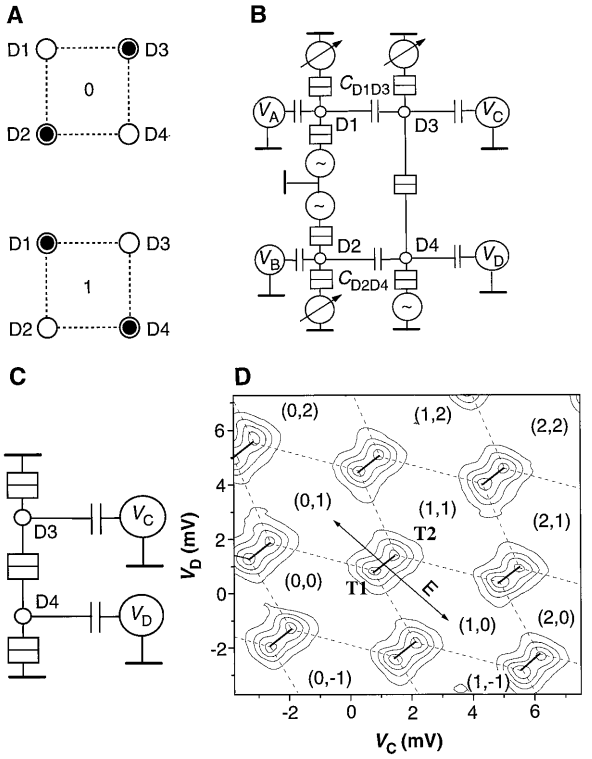

Fig. 1. (**A**) QCA cell showing two possible polarizations. (**B**) Schematic diagram of the experiment. (**C**) Double-dot system with two metal islands connected by a tunnel junction. V_C and V_D are gate voltages controlling the charge on dots D3 and D4. (**D**) Contour plot of measured conductance through the double dot as a function of gate voltages V_C and V_D, where (n_3, n_4) is the number of excess electrons on dots D3 and D4.

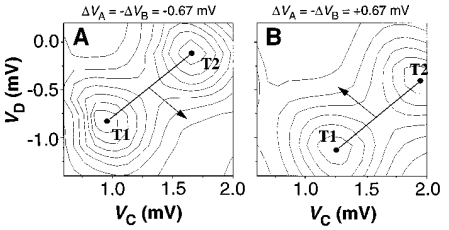

Fig. 2. Charging diagram of output double dot with $\Delta V_A = -\Delta V_B = -0.67$ mV (**A**) and $\Delta V_A = -\Delta V_B = +0.67$ mV (**B**). These values correspond to the maximum shift of the honeycomb (Fig. 1D) induced by an electron transfer in input dots. Arrows show the direction of honeycomb motion.

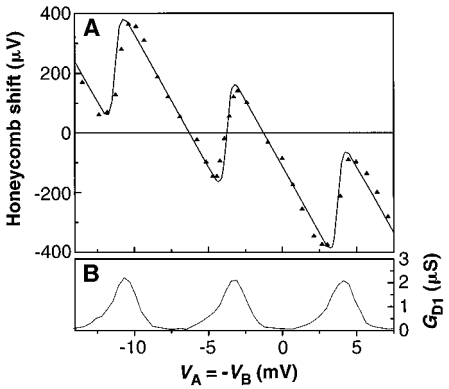

Fig. 3. (**A**) Experimental (▲) and theoretical (—) honeycomb shift as a function of driver voltages $V_A = -V_B$. Electron exchange occurs when the border crosses zero. Theory uses a temperature of 50 mK. (**B**) Conductance through input dot D1 as a function of driver voltage.

marking a region where a particular configuration (n_3, n_4) is the ground state, with n_3 and n_4 representing the number of excess electrons on islands D3 and D4, respectively. A switch of an electron between the two dots occurs along direction E, whereas total charge on the double dot remains constant along that direction.

To accomplish a polarization switch of a QCA cell, an electron transfer between the input dots must produce an opposite transfer of an electron between the output dots. The gate biases for the double dot set the working point V_C^0, V_D^0 to the center of the transition border (T1–T2) in the absence of an input signal. The cell is then in its most symmetrical state, and in the absence of an input signal the two polarizations are equally probable. An input "push-pull" signal ($+\Delta V_A = -\Delta V_B$) added to the driver gates polarizes the input dots, which in turn polarizes the output double dot. A polarization change in the output double dot corresponds to a movement of the entire honeycomb pattern along direction E relative to a fixed working point V_C^0, V_D^0. Electron switching in the output double dot takes place each time the border (T1–T2) crosses the working point. The ability to produce and detect a polarization switch of the output dots, induced by a single electron transfer in the input dots, demonstrates a functioning QCA cell.

In this experiment, we determined the charge state of the output double dot by measuring its conductance, which required a sweep of V_C and V_D. To prevent these voltages from affecting the input dots as a result of parasitic capacitance, we applied cancelation voltages, with polarities opposite to V_C and V_D, to gates A and B.

Although the input dots were not connected by a tunneling junction (Fig. 1B), by carefully controlling the charge on dots D1 and D2 we duplicated the behavior of the input double dot of a full four-dot QCA cell. We could not actually switch an electron between the input dots, but, by applying biases with opposite polarities to gates A and B, each time an electron was removed from one input dot, an electron was added to the other, mimicking an electron transfer in an input double dot. The advantages of having two separate dots as an input stage of a QCA cell are that each dot can be individually measured and the charge of each dot can be individually controlled. In this way, addition and removal of electrons in the input dots were easily synchronized during scan of the drivers.

As mentioned above, transfer of an electron between input dots produces a shift of the entire charging diagram of the output double dot along direction E. To observe this shift, "snapshots" of the conductance $G_{\text{double dot}}(V_C, V_D)$ were taken for different push-pull ($+\Delta V_A = -\Delta V_B$) settings on the drivers. The potential on a metal dot in the Coulomb blockade regime changes linearly as a function of gate voltage, with an abrupt shift when the electron population of the dot changes (6). Thus, the potentials on the input dots oscillate in a sawtooth pattern with driver voltage, resulting in sawtooth-like shifts of the honeycomb. We observed a slow shift of the border corresponding to a gradual increase of the potential on the input dots followed by an abrupt "reset." Two snapshots were taken at the extremes of the shift with an amplitude of ~370 μV (Fig. 2).

We measured the shift of the honeycomb border while sweeping gates A and B over a voltage that was sufficient for several electrons to transfer between the input dots. The measured border shift with respect to a fixed working point V_C^0, V_D^0 as a function of the driver voltage ($+V_A$ and $-V_B$) is shown in Fig. 3A. A periodic abrupt shift in the border position occurred each time an electron switched in the input dots [indicated by peaks in conductance through the input dots (Fig. 3B)], confirming that the shift was due to a single electron transfer. A parasitic cou-

pling from gates A and B to the output dots added a monotonic term to the border shift, but its magnitude was smaller than that of the periodic shift over the voltage range of one electron switch in the input dots.

We compared the observed border shift with theoretical results (Fig. 3A), which include cancelation voltages and all experimentally determined capacitances. The theoretical results were obtained by minimizing the classical electrostatic energy for the array of islands and voltage leads. The full-capacitance matrix was included, and the minimum energy charge configuration was calculated subject to the condition that island charge be an integer multiple of electronic charge. Finite temperature effects were obtained by thermodynamic averaging over all nearby charge configurations. Experiment and theory match very well with only the substrate background charge and temperature as fitting parameters. The background charge adds a random offset to the position of the border but does not change the magnitude or period of the observed shift. The best fit to experiment is obtained for a temperature of 50 mK. The discrepancy between this and the base temperature of the dilution refrigerator (15 mK) most likely occurs because of heating of the electron subsystem by electromagnetic and thermal noise sources (*7*) and the applied 4-μV excitation. This effect is common in transport experiments at temperatures below 100 mK (*6, 7*).

To show that the observed border shift represents a polarization switch of the cell at finite temperature, we combined the results of the border-shift measurements (Fig. 3) with measurements of the electrostatic potentials of the double dot. The electrostatic potential of each dot in the double dot was measured with the same device but with D1 and D2 as electrometers (*8*). The result is shown in Fig. 4A, where we plot electrostatic potential on dot D3 as measured by electrometer D1, together with theoretical calculations of the same potential at 0 and 50 mK, as a function of driver voltage V_A. The calculated excess charge on islands D3 and D4 of the double dot at 50 mK and, for reference, the charge on D3 at 0 K are indicated in Fig. 4B. Charge switching occurs at $V_A \sim -3.8$ mV, corresponding to an electron switch in the input dots. An input voltage swing $\Delta V_A = -\Delta V_B$ of 1.3 mV is sufficient for nearly complete transfer of an electron from one output dot to the other. An increase in coupling capacitance $C_{D1D3} = C_{D2D4}$ would lead to a more complete electron transfer, as shown in the theoretical plot (Fig. 4C), where we set the coupling capacitance to be equal to a junction capacitance. The data of Fig. 4 confirm that the experimentally observed honeycomb shift represents the polarization change of a functioning QCA cell.

The QCA architecture is a break from the FET-based paradigm of digital logic. Logic levels are encoded no longer as voltages on capacitors, which must be charged and discharged by current switches, but rather as the positions of electrons within a cell. The scalability of QCA offers the future possibility of functional devices that, at the molecular level, can operate at room temperature.

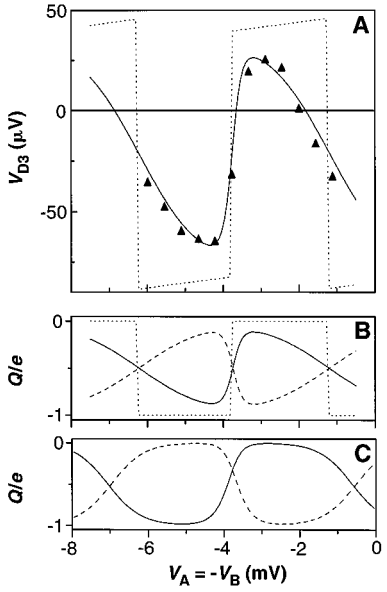

Fig. 4. (**A**) Voltage on dot D3 of output double dot as a function of driver voltage $V_A = -V_B$. Triangles are experimental data, and solid line represents theoretical values at 50 mK. For reference, theoretical data at 0 K (dotted line) are shown. (**B**) Calculated charge on dots D3 and D4 as a function of driver voltage for $C_{D1D2} = C_{D2D4} = 0.65$ *e*/mV (experimental value). Solid line represents charge on dot D3 at 50 mK, dashed line is charge on dot D4 at 50 mK, and dotted line is charge on D3 at 0 K. (**C**) Calculated charge on dots D3 and D4 as a function of driver voltage for $C_{D1D2} = C_{D2D4} = C_{junction} = 2.1$ *e*/mV. Solid line is charge on dot D3 at 50 mK, and dashed line is charge on dot D4 at 50 mK.

REFERENCES AND NOTES

1. C. S. Lent, P. D. Tougaw, W. Porod, G. H. Bernstein, *Nanotechnology* **4**, 49 (1993); C. S. Lent and P. D. Tougaw, *Proc. IEEE,* **85**, 541 (1997).
2. K. K. Likharev, *IBM J. Res. Dev.* (January 1988), p. 114.
3. P. D. Tougaw and C. S. Lent, *J. Appl. Phys.* **75**, 1818 (1994).
4. T. A. Fulton and G. H. Dolan, *Phys. Rev. Lett.* **58**, 109 (1987).
5. H. Pothier *et al.*, *Physica B* **169**, 573 (1991).
6. P. Lafarge *et al.*, *Z. Phys. B* **85**, 327 (1991).
7. D. Vion *et al.*, *J. Appl. Phys.* **77**, 2519 (1995).
8. I. Amlani, A. O. Orlov, G. L. Snider, G. H. Bernstein, unpublished results.

9. Supported in part by Defense Advanced Research Project Agency, Office of Naval Research (grant N00014-95-1-1166), and NSF. We thank W. Porod and J. Merz for useful discussions.

15 May 1997; accepted 23 June 1997

Structure, Bonding, and Geochemistry of Xenon at High Pressures

Wendel A. Caldwell, Jeffrey H. Nguyen, Bernd G. Pfrommer, Francesco Mauri, Steven G. Louie, Raymond Jeanloz

Although xenon becomes metallic at pressures above about 100 gigapascals, a combination of quantum mechanical calculations and high pressure–temperature experiments reveals no tendency on the part of xenon to form a metal alloy with iron or platinum to at least 100 to 150 gigapascals. The transformation of xenon from face-centered cubic (fcc) to hexagonal close-packed (hcp) structures is kinetically hindered, the differences in volume and bulk modulus between the two phases being smaller than we can resolve (less than 0.3 percent and 0.6 gigapascals, respectively). The equilibrium fcc-hcp phase boundary is at 21 (±3) gigapascals, which is a lower pressure than was previously thought, and it is unlikely that Earth's core serves as a reservoir for primordial xenon.

Like the other noble elements, Xe is characterized by a reluctance to form chemical bonds. Indeed, chemical inertness makes the noble gases useful as tracers that help reveal the evolution of planetary atmospheres and interiors (*1*–*6*). That Xe can bond to form compounds (*7*–*9*) and even, at high pressures, a hexagonal close-packed (hcp) metal (*10*–*12*), opens up the possibility that geochemical trends of the planets' noble gas abundances can be influenced by chemical reactions taking place at the elevated pressures and temperatures of planetary interiors. Specifically, the relative depletion of Earth's atmospheric Xe compared with meteoritic and solar abundances—the geochemical "missing Xe" problem (*2, 13, 14*)—suggests that significant amounts of Earth's primordial Xe could be sequestered at depth,